

Mathematical Model of Contractile Ring-Driven Cytokinesis in a Three-Dimensional Domain

Seunggyu Lee¹

Received: 18 April 2017 / Accepted: 5 January 2018
© Society for Mathematical Biology 2018

Abstract In this paper, a mathematical model of contractile ring-driven cytokinesis is presented by using both phase-field and immersed-boundary methods in a three-dimensional domain. It is one of the powerful hypotheses that cytokinesis happens driven by the contractile ring; however, there are only few mathematical models following the hypothesis, to the author's knowledge. I consider a hybrid method to model the phenomenon. First, a cell membrane is represented by a zero-contour of a phase-field implicitly because of its topological change. Otherwise, immersed-boundary particles represent a contractile ring explicitly based on the author's previous work. Here, the multi-component (or vector-valued) phase-field equation is considered to avoid the emerging of each cell membrane right after their divisions. Using a convex splitting scheme, the governing equation of the phase-field method has unique solvability. The numerical convergence of contractile ring to cell membrane is proved. Several numerical simulations are performed to validate the proposed model.

Keywords Cytokinesis · Contractile ring · Phase-field · Immersed-boundary

1 Introduction

Although cell division is one of the most fundamental and important phenomena of living cells, its general principles are still not clear because of its complicated process (Pollard and Cooper 2008). A plausible hypothesis of the division is that the formation of a contractile ring (CR) drives the physical division process by dragging the cell membrane (Shlomovitz and Gov 2008) and there are many studies on the

✉ Seunggyu Lee
sglee89@nims.re.kr

¹ National Institute for Mathematical Sciences, Daejeon 34047, Republic of Korea

function of a CR during the final step of cell division (called cytokinesis) (Bathe and Chang 2010; Bi et al. 1998; Calvert et al. 2011; Carvalgo and Oegema 2009; Celton-Morizur et al. 2004; Chang et al. 1997; Jochova et al. 1991; Kamasaki et al. 2007; Mandato and Berment 2001; Pelham and Chang 2002). However, assembly or dynamics of a CR in a cytokinesis is still poorly understood (Wang 2008). It is important to come up with testable models to decipher detailed assembly and dynamics from the amount of experimental observation or data. For example, biologists have addressed the experimental results of the relationship between cytokinesis and cancer cells (Daniels et al. 2004; Gisselsson et al. 2010; Kang et al. 2010) and it could be extremely expensive in a temporal or financial aspect to test each undesirable case in a laboratory, whereas its difficulty can be resolved by establishing a reliable computational model. Vavylonis et al. (2008) considered a simple numerical model for assembly mechanism of the CR for cytokinesis by fission yeast using the Monte Carlo method. Zhou et al. (2015) studied spatially coordinate curvature-dependent septum assembly of a CR during fission yeast cytokineses. Recently, Koudehi et al. (2016) performed numerical simulations to show the effect of actin spherical confinement and cross-linking in CR formation, and Lee et al. (2016) proposed a numerical model for a CR in a three-dimensional domain using an immersed-boundary (IB) method comparing its numerical result with an experimental data.

The phase-field (PF) method, whose governing equation is the Cahn–Hilliard (CH) equation (Cahn and Hilliard 1958), is a useful mathematical tool to resolve an interfacial problem when topological changes occur, such as solidification dynamics (Wheeler et al. 1992), image inpainting (Bertozzi et al. 2007; Li et al. 2015), tumor growth (Chen et al. 2014), multi-phase fluid flows (Lee et al. 2016). A multi-component system of the CH equation was first generalized in the de Fontaini’s literature (1967). Lee and Kim considered a second-order accurate nonlinear difference scheme for generalized multi-component CH system (Lee and Kim 2008). Zhao and Wang Zhao and Wang (2016b, a) proposed cytokinesis models using the phase-field method with a contractile forcing term.

The IB method was originally developed by Peskin (Peskin 1972), and it has an advantage presenting flexible boundaries to move or change shapes in a complicated fashion. An elastic boundary problem has been simulated using the IB method, such as the dynamics of a bent and twisted rod (Lim et al. 2008; Lim 2010), a deformable fiber (Vahidkhal and Abdollahi 2012), a wall modeling (Chen et al. 2014; Posa and Balaras 2014), and fluid flows between eccentric rotating cylinders (Botella et al. 2015).

In this paper, a process of contractile ring-driven cytokinesis is modeled by using PF and IB methods in a three-dimensional domain. The CR is represented by the Lagrangian particles using the IB method based on Lee et al. (2016) without a point-deleting algorithm. However, the IB method has a numerical difficulty when the boundaries suffer the topological changes like emerging or division; therefore, the PF method is used to describe the dynamics of the cell membrane because the topological change, cell division, is more easily described than using the IB method fully. To avoid merging the divided cell membranes again, the vector-valued CH systems are considered rather than the original CH equation.

The rest of the paper is organized as follows: The governing equations and their properties are introduced in Sect. 2. The discretization of the equations and numer-

ical solutions are given in Sect. 3. The simulation results are shown in Sect. 4. The conclusion is drawn in Sect. 5.

2 Mathematical Model

A contractile ring and a cell membrane are considered by using the IB and PF methods, respectively, in a three-dimensional incompressible fluid. Here, the incompressible fluid can be modeled by the Navier–Stokes equation as explained in the later section.

2.1 Fluid Motion

The cytokinesis is accomplished by a CR assembling just beneath the plasma membrane and contracting to divide one mother cell into two daughter cells. Concurrently, a new membrane is inserted into the plasma membrane by the fusion of intracellular vesicles (Alberts et al. 2002). Since describing the above processes exactly is too complicated in a modeling, the cell surface is modeled by the fluid interface for simplicity (Li and Kim 2016). The equations of fluid motion are given as

$$\frac{\partial \mathbf{u}}{\partial t} + \mathbf{u} \cdot \nabla \mathbf{u} = -\nabla p + \frac{1}{Re} \Delta \mathbf{u} + \frac{1}{We} \mathbf{f}, \quad \text{in } \Omega \times (0, \infty), \tag{1}$$

$$\nabla \cdot \mathbf{u} = 0, \tag{2}$$

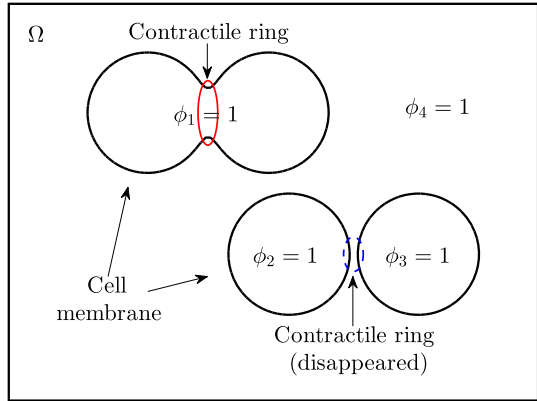
where $\mathbf{u}(\mathbf{x}, t) = (u(\mathbf{x}, t), v(\mathbf{x}, t), w(\mathbf{x}, t))$ is the fluid velocity, $\mathbf{x} = (x, y, z)$ is the Cartesian coordinate in $\Omega = (a_x, b_x) \times (a_y, b_y) \times (a_z, b_z) \subset \mathbb{R}^3$, t is the time variable, $p(\mathbf{x}, t)$ is the pressure, $Re = \rho U^* L^* / \eta$ is the Reynolds number, and $We = \rho (U^*)^2 L^* / \sigma$ is the Weber number with the density ρ , the viscosity η , the force density coefficient σ , the characteristic velocity U^* , and the characteristic length L^* . Here, the periodic boundary condition is implemented. $\mathbf{f} = (f^x(\mathbf{x}, t), f^y(\mathbf{x}, t), f^z(\mathbf{x}, t))$ is the fluid force density defined by $\mathbf{f}_m + \mathbf{f}_r$ with the force densities \mathbf{f}_m and \mathbf{f}_r generated by the cell membrane and the contractile ring, respectively.

2.2 Cell Membrane

For a lipid membrane, its elasticity is governed by the Helfrich free energy functional expressed by curvatures of the membrane (Helfrich 1973) and it is known that the bending energy given by the Helfrich Hamiltonian can be derived from the Landau–Ginzburg model (Gompper and Zschoke 1991). Note that the Landau–Ginzburg free energy functional leads to the CH equation on a solution conserved space. Therefore, the shape of the cell membranes is described by a zero-contour of a diffused-interface PF function $\phi(\mathbf{x}, t) = (\phi_1(\mathbf{x}, t), \phi_2(\mathbf{x}, t), \dots, \phi_N(\mathbf{x}, t))$, governed by the advective N -component CH equation (Lee et al. 2016):

$$\frac{\partial \phi_i}{\partial t} + \mathbf{u} \cdot \nabla \phi_i = \frac{1}{Pe} \Delta \left(f(\phi_i) - \epsilon^2 \Delta \phi_i + \beta(\phi) \right), \quad \text{for } i = 1, 2, \dots, N, \tag{3}$$

Fig. 1 Schematic illustration for the distribution of $\phi(\mathbf{x}, t)$ when $N = 4$



where ϕ_i is the volume fraction (here $\phi_i = 1$ in i th component and $\phi_i = -1$ in other components. See Fig. 1), $Pe = L^*U^*/M$ is the Peclet number with the mobility M , $f(\phi_i) = \phi_i^3 - \phi_i$, ϵ is the constant related to the interface thickness, and $\beta(\phi) = -\sum_{i=1}^N f(\phi_i)/N$ is the Lagrangian multiplier. Here, $\beta(\phi)$ makes $\sum_{i=1}^N \phi_i = 2 - N$ and it implies that ϕ_N can be decided without solving (3). The periodic boundary condition is also implemented as the fluid velocity field. The force density \mathbf{f}_m is defined as the surface tension force of ϕ_i written in the form (Kim 2005)

$$\mathbf{f}_m(\mathbf{x}, t) = - \sum_{i=1}^{N-1} \frac{\alpha \epsilon}{We} \nabla \cdot \left(\frac{\nabla \phi_i}{|\nabla \phi_i|} \right) |\nabla \phi_i| \nabla \phi_i, \tag{4}$$

where α is the correction coefficient for a diffused-interface model.

2.3 CR

The CR generates the constricting force to divide a cell into two cells during cytokinesis by creating a cleavage furrow (Miller 2011). For simplicity, I consider a CR as a certainly elastic shrinking loop as in my previous result (Lee et al. 2016). The evolution equation of the CR positions, defined as Lagrangian variables $\mathbf{X}_i(s_i, t) = (X_i(s_i, t), Y_i(s_i, t), Z_i(s_i, t))$ for $i = 1, \dots, N - 1$ with parameters s_i in $[0, L_{i,t}]$, where $L_{i,t}$ is the unstressed length of the i th ring, is given by

$$\frac{\partial \mathbf{X}_i(s_i, t)}{\partial t} = \mathbf{U}_i(s_i, t) = \int_{\Omega} (-\phi_i(\mathbf{x}, t)) \mathbf{u}(\mathbf{x}, t) \delta(\mathbf{x} - \mathbf{X}_i(s_i, t)) d\mathbf{x}, \tag{5}$$

where $\mathbf{U}_i(s, t)$ is the i th CR velocity on $\mathbf{X}_i(s_i, t)$ and $\delta(\mathbf{x})$ is the three-dimensional Dirac delta function. Here, the term $(-\phi_i(\mathbf{x}, t))$ makes the CR position on the cell membrane. In the model, the elastic force for the CR is generated by reducing $L_{i,t}$ as time evolves and the force density \mathbf{f}_r is defined as the following integration

$$\mathbf{f}_r(\mathbf{x}, t) = \sum_{i=1}^{N-1} \int_0^{L_{i,t}} \mathbf{F}_{r,i}(s_i, t) \delta(\mathbf{x} - \mathbf{X}_i(s_i, t)) ds, \tag{6}$$

where $\mathbf{F}_{r,i}(s_i, t) = \partial [T_i(s_i, t)\boldsymbol{\tau}_i(s_i, t)]/\partial s$ is the elastic force density of the i th CR, $T_i(s_i, t) = \sigma (|\partial\mathbf{X}_i/\partial s_i| - 1)$ is the tension of the i th CR, and $\boldsymbol{\tau}_i(s_i, t) = (\partial\mathbf{X}_i/\partial s_i)/|\partial\mathbf{X}_i/\partial s_i|$ is the unit tangent vector to the i th CR. The detailed descriptions can be referred in Lee et al. (2016).

2.4 Cell Growth

To model a series of cell divisions, a growth term of the cell should be added in (3) between each cytokinesis. In a tumor growth model (Britton 2003), a growth term is considered as

$$\rho_t(\mathbf{x}, t) + \nabla \cdot [\rho(\mathbf{x}, t)\mathbf{u}(\mathbf{x}, t)] = \lambda_p \rho(\mathbf{x}, t), \quad \text{in } \Omega_t, \tag{7}$$

where $\rho(\mathbf{x}, t)$ is the tumor density, λ_p is the proliferation rate, and Ω_t is the tumor domain. Furthermore, Eq. (7) can be written as

$$\nabla \cdot \mathbf{u}(\mathbf{x}, t) = \lambda_p, \quad \text{in } \Omega_t, \tag{8}$$

with the constant density of the tumor, i.e., $\rho(\mathbf{x}, t) \equiv \rho_0$. Applying (8) to a PF model (3), the result is

$$\begin{aligned} \frac{\partial \phi_i}{\partial t} + \mathbf{u} \cdot \nabla \phi_i &= \frac{1}{Pe} \Delta \left(f(\phi_i) - \epsilon^2 \Delta \phi_i + \beta(\boldsymbol{\phi}) \right) + \frac{\lambda}{2} (1 + \phi_i), \\ \text{for } i &= 1, 2, \dots, N - 1, \end{aligned} \tag{9}$$

where

$$\lambda = \begin{cases} \lambda_p, & \text{in a cell growth level} \\ 0, & \text{otherwise.} \end{cases}$$

3 Numerical Method

First, the discretization of each variable is introduced before considering numerical solvers for governing equations. Let the set of cell-centered grid points $\Omega_h = \{(x_j, y_k, z_l) : x_j = (j - 0.5)h, y_k = (k - 0.5)h, z_l = (l - 0.5)h\}$ be the phase-field computational domain for $j = 1, \dots, N_x, k = 1, \dots, N_y$, and $l = 1, \dots, N_z$, where $h = (b_x - a_x)/N_x = (b_y - a_y)/N_y = (b_z - a_z)/N_z$ is the uniform spatial step size with the numbers of points N_x, N_y , and N_z in x -, y -, and z -directions, respectively. Let $\phi_i(\mathbf{x}, t)$ and $p(\mathbf{x}, t)$ approximate on Ω_h by denoting $\phi_i(x_j, y_k, z_l, n\Delta t)$ and $p(x_j, y_k, z_l, n\Delta t)$ as $\phi_{i,jkl}^n$ and p_{jkl}^n , respectively, where n is the integer and Δt is the spatial step size. Similarly, let \mathbf{u} approximate as $(u_{j+\frac{1}{2},kl}, v_{j,k+\frac{1}{2},l}, w_{jk,l+\frac{1}{2}})$ on cell-edged points (called a marker-and-cell (MAC) mesh; Harlow and Welch 1965) (See

Fig. 2 Schematic of a grid and variables

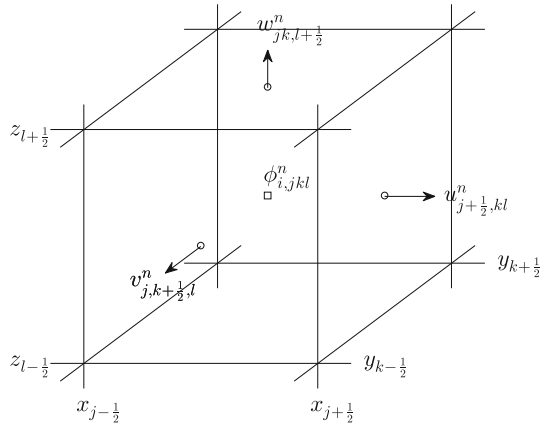


Fig. 3 Schematic of parametrization of $\mathbf{X}(s, t)$. To simplify, the phase index i is omitted in this figure

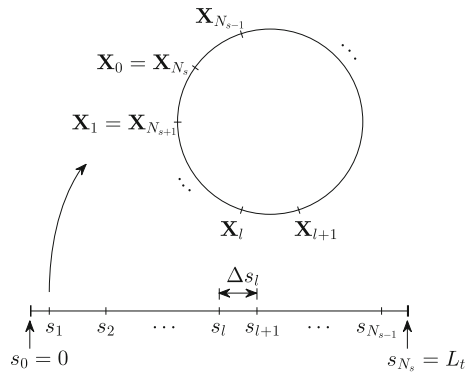


Fig. 2). The notations ϕ^n, \mathbf{u}^n are used when approximating only along the temporal axis.

Moreover, let $\Delta s_{i,m}^n$ be the time-dependent step size satisfying $L_{i,t} = \sum_{m=0}^{N_{i,s}-1} \Delta s_{i,m}^n = \alpha_i(t^n)L_i, 0$, where $N_{i,s}$ is the number of i th variable intervals, $\alpha_i(t^n)$ is a scaling factor function at time $t = t^n$, and $L_{i,0}$ is the initial length of the i th CR. Then, $s_{i,m}^n = 0$ and $s_{i,m+1}^n = s_{i,m}^n + \Delta s_{i,m}^n$ for $m = 0, \dots, N_{i,s} - 1$. The discrete i th CR position is defined as $\mathbf{X}_{i,m}^n = \mathbf{X}(s_{i,m}^n, n\Delta t) = (X_i^n, Y_i^n, Z_i^n)$ for $m = 1, \dots, N_{i,s}$. Note that $\mathbf{X}_{i,0}^n = \mathbf{X}_{i,N_{i,s}}^n$ and $\mathbf{X}_{i,N_{i,s}+1}^n = \mathbf{X}_1^n$ because of the periodicity. This parametrization of $\mathbf{X}_i(s_i, t)$ is schematically illustrated in Fig. 3.

Next, the discrete operators are defined. The discrete gradient operator ∇_d is defined as

$$\nabla_d \phi_{jkl}^n = \left(\frac{\phi_{j+1/2,kl}^n - \phi_{j-1/2,kl}^n}{h}, \frac{\phi_{j,k+1/2,l}^n - \phi_{j,k-1/2,l}^n}{h}, \frac{\phi_{jk,l+1/2}^n - \phi_{jk,l-1/2}^n}{h} \right),$$

and the discrete divergence operator $\nabla_d \cdot \phi_{ijk}^n$ is defined as

$$\nabla_d \cdot \phi_{jkl}^n = \frac{\phi_{j+\frac{1}{2},kl}^n - \phi_{j-\frac{1}{2},kl}^n + \phi_{j,k+\frac{1}{2},l}^n - \phi_{j,k-\frac{1}{2},l}^n + \phi_{jk,l+\frac{1}{2}}^n - \phi_{jk,l-\frac{1}{2}}^n}{h}$$

From the above operators, the discrete Laplacian operator Δ_d is defined as

$$\begin{aligned} \Delta_d \phi_{jkl}^n &= \nabla_d \cdot (\nabla_d \phi_{jkl}^n) \\ &= \frac{\phi_{j+1,kl}^n + \phi_{j-1,kl}^n + \phi_{j,k+1,l}^n + \phi_{j,k-1,l}^n + \phi_{jk,l+1}^n + \phi_{jk,l-1}^n - 6\phi_{jkl}^n}{h^2} \end{aligned}$$

These operators are also applied to $u_{i+\frac{1}{2},jk}^n$, $v_{i,j+\frac{1}{2},k}$, or $w_{ij,k+\frac{1}{2}}$ in a similar manner.

3.1 Fluid Motion

First, \mathbf{u}^{n+1} is updated from a given \mathbf{u}^n . Applying the explicit scheme, the time-discrete version of Eqs. (1) and (2) is written as follows:

$$\frac{\mathbf{u}^{n+1} - \mathbf{u}^n}{\Delta t} + \mathbf{u}^n \cdot \nabla \mathbf{u}^n = -\nabla p^{n+1} + \frac{1}{Re} \Delta \mathbf{u}^n + \frac{1}{We} \mathbf{f}^n, \tag{10}$$

$$\nabla \cdot \mathbf{u}^{n+1} = 0. \tag{11}$$

Next, the Chorin’s projection method (Chorin 1968), well known as a useful solver for the Navier–Stokes equation, is used:

Step 1 Calculate the temporal velocity $\tilde{\mathbf{u}}$ by solving the following equation:

$$\frac{\tilde{\mathbf{u}} - \mathbf{u}^n}{\Delta t} = -\mathbf{u}^n \cdot \nabla \mathbf{u}^n + \frac{1}{Re} \Delta \mathbf{u}^n + \frac{1}{We} \mathbf{f}^n. \tag{12}$$

Note that $\tilde{\mathbf{u}}$ could not be divergence-free. Equation (12) can be discretized in space as follows:

$$\begin{aligned} \frac{\tilde{u}_{j+\frac{1}{2},kl} - u_{j+\frac{1}{2},kl}^n}{\Delta t} &= -(\mathbf{u} \cdot \nabla_d u)_{j+\frac{1}{2},kl}^n + \frac{1}{Re} \Delta_d u_{j+\frac{1}{2},kl}^n + \frac{1}{We} f_{j+\frac{1}{2},kl}^{x,n}, \\ \frac{\tilde{v}_{j,k+\frac{1}{2},l} - v_{j,k+\frac{1}{2},l}^n}{\Delta t} &= -(\mathbf{u} \cdot \nabla_d v)_{j,k+\frac{1}{2},l}^n + \frac{1}{Re} \Delta_d v_{j,k+\frac{1}{2},l}^n + \frac{1}{We} f_{j,k+\frac{1}{2},l}^{y,n}, \\ \frac{\tilde{w}_{jk,l+\frac{1}{2}} - w_{jk,l+\frac{1}{2}}^n}{\Delta t} &= -(\mathbf{u} \cdot \nabla_d w)_{jk,l+\frac{1}{2}}^n + \frac{1}{Re} \Delta_d w_{jk,l+\frac{1}{2}}^n + \frac{1}{We} f_{jk,l+\frac{1}{2}}^{z,n}. \end{aligned}$$

Here, the advection terms are computed with the upwind scheme. The details can be seen in Lee et al. (2016).

Step 2 Update \mathbf{u}^{n+1} using $\tilde{\mathbf{u}}$.

$$\frac{\mathbf{u}^{n+1} - \tilde{\mathbf{u}}}{\Delta t} = -\nabla p^{n+1}. \tag{13}$$

Equation (13) can be discretized in space as follows:

$$\begin{aligned} \frac{u_{j+\frac{1}{2},kl}^{n+1} - \tilde{u}_{j+\frac{1}{2},kl}}{\Delta t} &= -\frac{p_{j+1,kl}^{n+1} - p_{jkl}^{n+1}}{h}, \\ \frac{v_{j,k+\frac{1}{2},l}^{n+1} - \tilde{v}_{j,k+\frac{1}{2},l}}{\Delta t} &= -\frac{p_{j,k+1,l}^{n+1} - p_{jkl}^{n+1}}{h}, \\ \frac{w_{jk,l+\frac{1}{2}}^{n+1} - \tilde{w}_{jk,l+\frac{1}{2}}}{\Delta t} &= -\frac{p_{jk,l+1}^{n+1} - p_{jkl}^{n+1}}{h}. \end{aligned}$$

Here, the pressure field can be calculated by solving the Poisson equation:

$$\Delta p^{n+1} = \frac{1}{\Delta t} (\nabla_d \cdot \tilde{\mathbf{u}}). \tag{14}$$

Note that it is derived from (13) applying the divergence operator ($\nabla_d \cdot$) and the condition (11). Here, the multi-grid (Trottenberg et al. 2001) is used to solve (14) with V-cycles and Gauss–Seidel relaxation. See Lee et al. (2016).

3.2 Cell Membrane

Here, the numerical solver for the cell membrane equation is described with its growth term (9). Based on the convex splitting scheme of Eyre’s work (1998), Eq. (9) can be discretized in time as follows:

$$\begin{aligned} \frac{\phi_i^{n+1} - \phi_i^n}{\Delta t} + \mathbf{u}^n \cdot \nabla \phi_i^n &= \frac{1}{Pe} \Delta \left((\phi_i^{n+1})^3 - \phi_i^n - \epsilon^2 \Delta_d \phi_i^{n+1} + \beta(\phi^n) \right) \\ &\quad + \frac{\lambda}{2} (1 + \phi_i^n). \end{aligned}$$

for $i = 1, 2, \dots, N - 1$. (15)

Theorem 1 Equation (15) is unconditionally uniquely solvable for each i .

Proof To simplify the notation, let us omit the index i in a proof. Consider the following functional

$$\begin{aligned} \mathcal{F}(\phi) &= \frac{1}{2\Delta t} \|\phi - \phi^n\|_{-1,h}^2 + \langle \mathbf{u}^n \cdot \nabla \phi^n, \phi \rangle_{-1,h} - \frac{\lambda}{2} \langle 1 + \phi^n, \phi \rangle_{-1,h} \\ &\quad + \frac{1}{Pe} \left(\frac{1}{4} \|\phi\|_4^4 - \langle \phi^n, \phi \rangle_2 + \frac{\epsilon^2}{2} \|\nabla \phi\|_2^2 + \langle \beta(\phi^n), \phi \rangle_2 \right), \end{aligned}$$

where $\langle \phi, \psi \rangle_p$ is the L_p -inner product, $\|\phi\|_p^2 = \langle \phi, \phi \rangle_p$ is the L_p -norm, $\langle \phi, \psi \rangle_{-1,h} = \langle -\Delta\phi, \psi \rangle_2$ is the inner product on a Hilbert space, and $\|\phi\|_{-1,h}^2 = \langle \phi, \phi \rangle_{-1,h}$ is the norm corresponding to the inner product. Then, its first variation is

$$\delta_\phi \mathcal{F}(\phi; \psi) = \left\langle \frac{\phi - \phi^n}{\Delta t} + \mathbf{u}^n \cdot \nabla \phi^n - \frac{1}{Pe} \Delta (\phi^3 - \phi^n - \epsilon^2 \Delta \phi + \beta(\phi^n)) - \frac{\lambda}{2} (1 + \phi^n), \psi \right\rangle_{-1,h},$$

and the second variation is

$$\delta_\phi^2 \mathcal{F}(\phi; \psi) = \frac{1}{\Delta t} \|\psi\|_{-1,h}^2 + \frac{3}{Pe} \|\phi\psi\|_2^2 + \frac{\epsilon^2}{Pe} \|\nabla\psi\|_2^2 > 0,$$

where ψ is in a Hilbert space $H = \{\phi : \int \phi = 0\}$. Since the second variation is strictly positive, \mathcal{F} is a strictly convex functional and it implies that Eq. (15) is a unique minimizer of \mathcal{F} from its first variation.

Here, spatial discretization is similarly defined as the previous section using ∇_d and Δ_d . The detailed descriptions of numerical solver and its stability are in Lee et al. (2012).

3.3 CR

Using the updated fluid velocity \mathbf{u}^{n+1} and PF functions $\phi^{n+1} = (\phi_1^{n+1}, \dots, \phi_N^{n+1})$ derived above, the CR velocity $\mathbf{U}_{i,m}^{n+1}$ and boundary position $\mathbf{X}_{i,m}^{n+1}$ are also updated by solving the following discrete equation:

$$\mathbf{U}_{i,m}^{n+1} = - \sum_{j=1}^{N_x} \sum_{k=1}^{N_y} \sum_{l=1}^{N_z} \phi_{i,jkl} \mathbf{u}_{jkl}^{n+1} \delta_h^3 (\mathbf{x}_{jkl} - \mathbf{X}_{i,m}^n) h^3, \tag{16}$$

$$\mathbf{X}_{i,m}^{n+1} = \mathbf{X}_{i,m}^n + \Delta t \mathbf{U}_{i,m}^{n+1}, \tag{17}$$

for $i = 1, \dots, N - 1$ and $m = 1, \dots, N_{i,s}$. Note that the motion of CR is calculated numerically when $\lambda = 0$ in Eq. 15 and the position of cell division in numerical simulation will be determined by the position of CR when the division occurs.

The following theorem proves the pointwise convergence of $\mathbf{X}_{i,m}^n$ to the zero-contours representing the cell membranes. To simplify the notation, the phase index i is omitted in the theorem. Moreover, assume that the PF function is fixed in time; hence, denote $\phi_{i,jkl}^n$ and $\mathbf{X}_{i,m}^n$ as ϕ_{jkl} and \mathbf{X}_m^n , respectively.

Theorem 2 *Given $\epsilon > 0$, $\|(x_\xi, y_\eta, z_\zeta) - \mathbf{X}_m^n\|_2 < \epsilon$ as $n \rightarrow \infty$ for some point (x_ξ, y_η, z_ζ) on $\{\mathbf{x} : \phi(\mathbf{x}) = 0\}$.*

Proof Since it could be straightforwardly extended to higher-order cases, consider the problem as an one-dimensional case. If $|X_m^n - x_\xi| < 2h$, take $\epsilon = 2h$. Otherwise, (16) and (17) are first rewritten by using the notation $u_j^{n+1} = 0.5 \left(u_{j+\frac{1}{2}}^{n+1} + u_{j-\frac{1}{2}}^{n+1} \right)$ as follows:

$$X_m^{n+1} = X_m^n - \Delta t \sum_{j=1}^{N_x} \phi_j u_j^{n+1} \delta_h(x_j - X_m^n) h,$$

or,

$$\frac{X_m^{n+1} - x_\xi}{X_m^n - x_\xi} = 1 - \frac{h \Delta t}{X_m^n - x_\xi} \sum_{j=1}^{N_x} \phi_j u_j^{n+1} \delta_h(x_j - X_m^n). \tag{18}$$

Without loss of generality, assume $u_j^{n+1} > 0$ because the CR always shrinks when the particle move happens. Clearly, h and Δt are positive and δ_h has compact support only on four points near X_m^n with a positive value. By compact supportedness, (18) is rewritten again as

$$\frac{X_m^{n+1} - x_\xi}{X_m^n - x_\xi} = 1 - \frac{h \Delta t}{X_m^n - x_\xi} \sum_{x_j \in [X_m^n - 2h, X_m^n + 2h]} \phi_j u_j^{n+1} \delta_h(x_j - X_m^n).$$

If $|X_m^n - x_\xi| \geq 2h$, then $(X_m^n - x_\xi)\phi_j > 0$ for $\{j : x_j \in [X_m^n - 2h, X_m^n + 2h]\}$. Moreover, it implies that

$$\left| \frac{X_m^{n+1} - x_\xi}{X_m^n - x_\xi} \right| < 1,$$

and the proof is over.

4 Simulation Results

In this section, several numerical tests are described to validate our modeling in a three-dimensional domain. First, Theorem 2 is checked numerically and then some numerical simulations are performed to show the configurations of cell membrane and CR. The computational domain will be set as $\Omega_h = (0, 1) \times (0, 1) \times (0, 2)$ unless otherwise stated. Except for comparing with experimental data, I refer the non-dimensional parameters in my previous results (Lee et al. 2016).

4.1 ϕ -Effect in IB Velocity

The first simulation is to prove the result of Theorem 2 numerically. The parameters are chosen as $N_x = N_y = 32$, $N_z = 64$, $Re = 10$, $We = 10$,

Fig. 4 Temporal evolution of differences between the radii of CR and cell membrane at $z = 0.5$ until the cytokinesis occurs

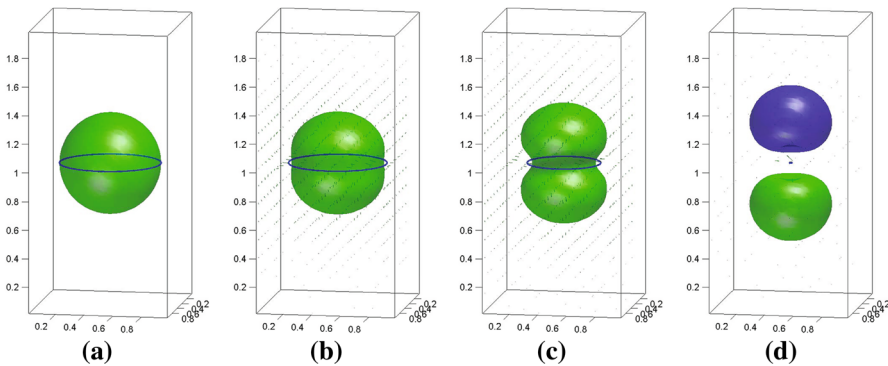
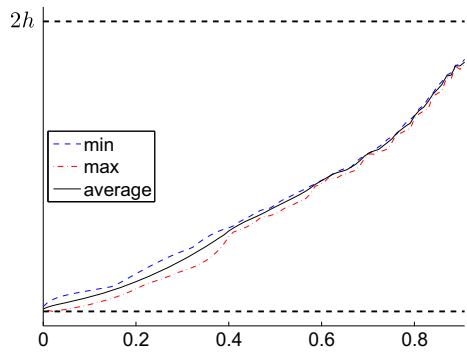


Fig. 5 Numerical results of cell division process starting with a single cell. The isosurfaces represent cells, the blue line is the CR, and arrows describe the fluid velocities. **a** Initial, **b** $t = 300\Delta t$, **c** $t = 600\Delta t$, **d** $t = 1000\Delta t$ (Color figure online)

$Pe = 1/\epsilon$, $\epsilon = \epsilon_3$, $\Delta t = 0.1Re \cdot h^2$, $L_0 = 2\pi(0.35)$, and $N_t = 1000$. Figure 4 shows the temporal evolution of differences between the radii of CR and cell membrane at $z = 0.5$ until the cytokinesis occurs. Here, the black bold dotted lines represent the upper($2h$) and lower(0) bounds in the hypothesis and the distances calculated from numerical results are drawn by thin lines. The distances are calculated at each Lagrangian particle. The legends min, max, and average in graph represent the minimum, maximum, and average distances, respectively. Since the differences are always bounded by $[0, 2h]$, it has a good agreement with Theorem 2.

4.2 Single Cell

Next, the numerical simulations of cell division process starting with a single cell are performed in this section. The isosurfaces represent cells, the blue line is the CR, and arrows describe the fluid velocities in Fig. 5. The same parameters as the previous simulation are chosen. Note that the topological change, i.e., cytokinesis, can be expressed by using the proposed model without complicated numerical treatment.

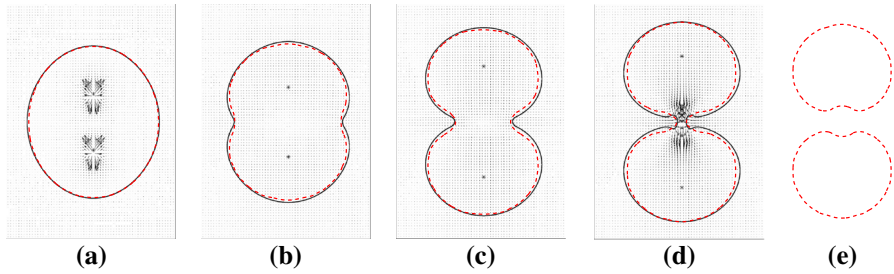


Fig. 6 Comparison of temporal evolution with Li's work (2012). The arrows and the black solid lines represent the velocity field and the cell membranes, respectively, in the background images, which are reprinted with permission from Springer (Li et al. 2012). Otherwise, the red dotted lines are a zero-contour of ϕ (Color figure online)

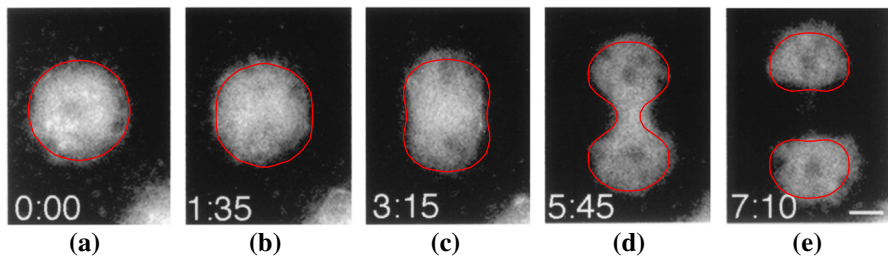


Fig. 7 Configuration of cell membranes from the numerical simulation and in vivo. Background images, reprinted with permission from National Academy of Sciences (Zang and Spudich 1998), and red solid lines represent the experimental data and the simulation results, respectively. **a** Initial, **b** $t = 0.2930$, **c** $t = 0.6006$, **d** $t = 1.0693$, **e** $t = 1.3184$ (Color figure online)

4.3 Comparison with Previous Model

Here, the numerical simulation for comparison with a previous model is considered to validate the proposed model. Li et al. (2012) proposed the mathematical model for simulating a single axisymmetric cell using an IB method. With the initial condition from the elongated cell in the Li's work, I perform the numerical simulation and its results are presented in Fig. 6. The arrows and the black solid lines represent the velocity field and the cell membranes, respectively, from the previous work. Otherwise, the red dotted lines are a zero-contour of ϕ . Note that there are no data for comparing with Fig. 6e because it is quite hard to perform the simulation after the cell is divided in the previous work.

4.4 Comparison with Experiment Data

Moreover, Fig. 7 shows the configuration of cell membranes from the numerical simulation and in vivo. Background images and red solid lines represent the experimental data and the simulation results, respectively. The used parameters are $N_x = N_y = 32$, $N_z = 64$, $Re = 15$, $We = 10$, $Pe = 1/\epsilon$, $\epsilon = \epsilon_3$, $\Delta t = 0.1 Re \cdot h^2$, $L_0 = 2\pi(0.25)$, and $N_t = 1000$. Note that computational parameters are chosen in order to match the

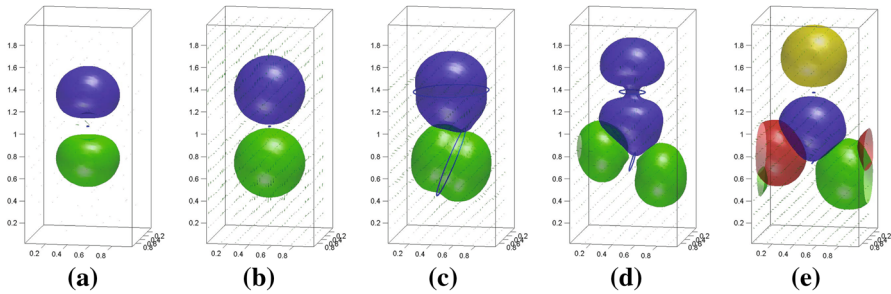


Fig. 8 Numerical results of cell division process starting with a multiple cell. The isosurfaces represent cells, the blue line is the CR, and arrows describe the fluid velocities. **a** $1000\Delta t$, **b** $1500\Delta t$, **c** $2000\Delta t$, **d** $2500\Delta t$, **e** $3000\Delta t$ (Color figure online)

numerical result and the experimental data since the exact values for the experience are unknown. The background images are *in vivo*, and the red solid lines present the simulation results. Note that the times in numerical simulations are non-dimensionalized in (a)–(e) and their ratios are well matched to experimental ones. As shown in the figure, the result shows that the experiment data can be approximated well by the proposed model.

4.5 Multiple Divisions

Now, the simulation with a series of divisions is considered in this subsection. The position of cell division will be randomly chosen on the cell membrane. The parameters are the same as the first simulation, except $N_t = 3000$. Figure 8 shows the numerical results of cell division process starting with a multiple cell. Because the temporal evolution is the same as one cell until $t = 1000\Delta t$, Fig. 8a starts with the state when $t = 1000\Delta t$. In Fig. 8b, the cell membrane is growing with $\lambda_p = 1$. The cell growth was already stopped, and the second cell division starts in Fig. 8c, and the cytokinesis keeps going in Fig. 8d. At last, Fig. 8e shows that four daughter cells exist after two divisions. If the usual CH equation, not the vector-valued one, is used to model, emerging should be happened in Fig. 8b or c because the distance between each two daughter cells is too close; however, it is resolved to use the vector-valued PF method.

5 Conclusion

Mathematical model of contractile ring-driven cytokinesis was proposed by using both PF and IB methods in this paper. To validate the model in a mathematical sense, we proved the solvability of the PF, governed the cell membrane and the convergence of the IB equation and governed the CR. Moreover, several numerical simulations were performed. The first result had a good agreement with the convergence theorem of CR, and it was also shown that the experimental data from Zang and Spudich (1998) can be approximated well by the proposed model. The multiple division simulation

result was also presented. In the future work, the nucleus division could be modeled by modifying the CH equation and more detailed theories in biology would be considered.

Acknowledgements The author was supported by the National Institute for Mathematical Sciences (NIMS) grant funded by the Korean government (No. A21300000) and the National Research Foundation of Korea (NRF) grant funded by the Korea government (MSIP) (No. 2017R1C1B1001937).

References

- Alberts B, Johnson A, Lewis J, Raff M, Roberts P (2002) Molecular biology of the cell, 4th edn. Garland Science, New York
- Bathe M, Chang F (2010) Cytokinesis and the contractile ring in fission yeast: towards a systems-level understanding. *Trends Microbiol* 18:38–45
- Bertozi A, Esedoglu S, Gilette A (2007) Inpainting of binary images using the Cahn–Hilliard equation. *IEEE Trans Image Process* 16:285–291
- Bi E, Maddox P, Lew D, Salmon E, McMilland E, Yeh E, Prihngle J (1998) Involvement of an actomyosin contractile ring in *Saccharomyces cerevisiae* cytokinesis. *J Cell Biol* 142:1301–1312
- Botella O, Ait-Messaoud M, Pertat A, Cheny Y, Rigal C (2015) The LS-STAG immersed boundary method for non-Newtonian flows in irregular geometries: flow of shear-thinning liquids between eccentric rotating cylinders. *Theor Comput Fluid Dyn* 29:93–110
- Britton N (2003) Essential mathematical biology. Springer, Berlin
- Cahn J, Hilliard J (1958) Free energy of a nonuniform system. I. Interfacial free energy. *J Chem Phys* 28(2):258–267
- Calvert M, Wright G, Lenong F, Chiam K, Chen Y, Jedd G, Balasubramanian M (2011) Myosin concentration underlies cell size-dependent scalability of actomyosin ring constriction. *J Cell Biol* 195:799–813
- Carvalgo A, Oegema ADK (2009) Structural memory in the contractile ring makes the duration of cytokinesis independent of cell size. *Cell* 137:926–937
- Celton-Morizur S, Dordes N, Fraissier V, Tran P, Paoletti A (2004) C-terminal anchoring of mid1p to membranes stabilized cytokinetic ring position in early mitosis in fission yeast. *Mol Cell Biol* 24:10621–10635
- Chang F, Drubin D, Nurse P (1997) cdc12p, a protein required for cytokinesis in fission yeast, is a component of the cell division ring and interacts with profilin. *J Cell Biol* 137:169–182
- Chen Y, Wise S, Shenoy V, Lowengrub J (2014a) A stable scheme for a nonlinear multiphase tumor growth model with an elastic membrane. *Int J Numer Methods Biomed Eng* 30(7):726–754
- Chen Z, Hickel S, Devesa A, Berland J, Adams N (2014b) Wall modeling for implicit large-eddy simulation and immersed-interface methods. *Theor Comput Fluid Dyn* 28(1):1–21
- Chorin A (1968) Numerical solution of the Navier–Stokes equation. *Math Comput* 22:745–762
- Daniels M, Wang Y, Lee M, Venkitaraman A (2004) Abnormal cytokinesis in cells deficient in the breast cancer susceptibility protein brca2. *Science* 306(5697):876–879
- de Fontaine D (1967) A computer simulation of the evolution of coherent composition variations in solid solutions. Ph.D. thesis, Northwestern University
- Eyer D (1998) Unconditionally gradient stable scheme marching the Cahn–Hilliard equation. *MRS Proc* 529:39–46
- Gisselsson D, Jin Y, Lindgren D, Persson J, Gisselsson L, Hanks S, Sehic D, Mengelbier L, Øra I, Rahman N et al (2010) Generation of trisomies in cancer cells by multipolar mitosis and incomplete cytokinesis. *Proc Natl Acad Sci* 107(47):20489–20493
- Gompper G, Zschoke S (1991) Elastic properties of interfaces in a Ginzburg–Landau theory of swollen micelles, droplet crystals and lamellar phases. *Europhys Lett* 16:731–736
- Harlow E, Welch J (1965) Numerical calculation of time dependent viscous incompressible flow with free surface. *Phys Fluid* 8:2182–2189
- Helfrich W (1973) Elastic properties of lipid bilayers: theory and possible experiments. *Z Naturforschung C* 28:693–703
- Jochova J, Rupes I, Streiblova E (1991) F-actin contractile rings in protoplasts of the yeast *Schizosaccharomyces*. *Cell Biol Int Rep* 15:607–610

- Kamasaki T, Osumi M, Mabuchi I (2007) Three-dimensional arrangement of f-actin in the contractile ring of fission yeast. *J Cell Biol* 178:765–771
- Kang B, Mackey M, El-Sayed M (2010) Nuclear targeting of gold nanoparticles in cancer cells induces dna damage, causing cytokinesis arrest and apoptosis. *J Am Chem Soc* 132(5):1517–1519
- Kim J (2005) A continuous surface tension force formulation for diffuse-interface models. *J Comput Phys* 204(2):784–804
- Koudehi M, Tang H, Vavylonis D (2016) Simulation of the effect of confinement in actin ring formation. *Biophys J* 110(3):126a
- Lee H, Kim J (2008) A second-order accurate non-linear difference scheme for the n-component Cahn–Hilliard system. *Physica A* 387:4787–4799
- Lee H, Choi J, Kim J (2012) A practically unconditionally gradient stable scheme for the n-component Cahn–Hilliard system. *Physica A* 391:1009–1019
- Lee S, Jeong D, Choi Y, Kim J (2016a) Comparison of numerical methods for ternary fluid flows: immersed boundary, level-set, and phase-field methods. *J KSIAM* 20(1):83–106
- Lee S, Jeong D, Lee W, Kim J (2016b) An immersed boundary method for a contractile elastic ring in a three-dimensional newtonian fluid. *J Sci Comput* 67(3):909–925
- Li Y, Kim J (2016) Three-dimensional simulations of the cell growth and cytokinesis using the immersed boundary method. *Math Biosci* 271:118–127
- Li Y, Yun A, Kim J (2012) An immersed boundary method for simulating a single axisymmetric cell growth and division. *J Math Biol* 65:653–675
- Li Y, Jeong D, Choi J, Lee S, Kim J (2015) Fast local image inpainting based on the local Allen–Cahn model. *Digital Signal Process* 37:65–74
- Lim S (2010) Dynamics of an open elastic rod with intrinsic curvature and twist in a viscous fluid. *Phys Fluids* 22(2):024104
- Lim S, Ferent A, Wang X, Peskin C (2008) Dynamics of a closed rod with twist and bend in fluid. *SIAM J Sci Comput* 31(1):273–302
- Mandato C, Berment W (2001) Contraction and polymerization cooperate to assemble and close actomyosin rings round xenopus oocyte wounds. *J Cell Biol* 154:785–797
- Miller A (2011) The contractile ring. *Curr Biol* 21:R976–R978
- Pelham R, Chang F (2002) Actin dynamics in the contractile ring during cytokinesis in fission yeast. *Nature* 419:82–86
- Peskin C (1972) Flow patterns around heart valves: a numerical method. *J Comput Phys* 10(2):252–271
- Pollard T, Cooper J (2008) Actin, a central player in cell shape and movement. *Science* 326:1208–1212
- Posa A, Balaras E (2014) Model-based near-wall reconstructions for immersed-boundary methods. *Theor Comput Fluid Dyn* 28(4):473–483
- Shlomovitz R, Gov N (2008) Physical model of contractile ring initiation in dividing cells. *Biophys J* 94:1155–1168
- Trottenberg U, Oosterlee C, Schüller A (2001) *Multigrid*. Academic Press, London
- Vahidkhal K, Abdollahi V (2012) Numerical simulation of a flexible fiber deformation in a viscous flow by the immersed boundary-lattice Boltzmann method. *Commun Nonlinear Sci Numer Simul* 17(3):1475–1484
- Vavylonis D, Wu J, Hao S, O’Shaughnessy B, Pollard T (2008) Assembly mechanism of the contractile ring for cytokinesis by fission yeast. *Science* 319:97–100
- Wang MZY (2008) Distinct pathways for the early recruitment of myosin ii and actin to the cytokinetic furrow. *Mol Biol Cell* 19(1):318–326
- Wheeler A, Boettinger W, McFadden G (1992) Phase-field model for isothermal phase transitions in binary alloys. *Phys Rev A* 45(10):7424–7439
- Zang J, Spudich J (1998) Myosin ii localization during cytokinesis occurs by a mechanism that does not require its motor domain. *Proc Natl Acad Sci* 95(23):13652–13657
- Zhao J, Wang Q (2016a) A 3d multi-phase hydrodynamic model for cytokinesis of eukaryotic cells. *Commun Comput Phys* 19(03):663–681
- Zhao J, Wang Q (2016b) Modeling cytokinesis of eukaryotic cells driven by the actomyosin contractile ring. *Int J Numer Methods Biomed Eng* 32(12):e027774
- Zhou Z, Munteanu E, He J, Ursell T, Bathe M, Huang K, Chang F (2015) The contractile ring coordinates curvature-dependent septum assembly during fission yeast cytokinesis. *Mol Biol Cell* 26(1):78–90